Molecular Cell, Volume *70*

Supplemental Information

An Optogenetic Platform for Real-Time, Single-Cell Interrogation of Stochastic Transcriptional Regulation

Marc Rullan, Dirk Benzinger, Gregor W. Schmidt, Andreas Milias-Argeitis, and Mustafa Khammash

Supplementary Figures

A

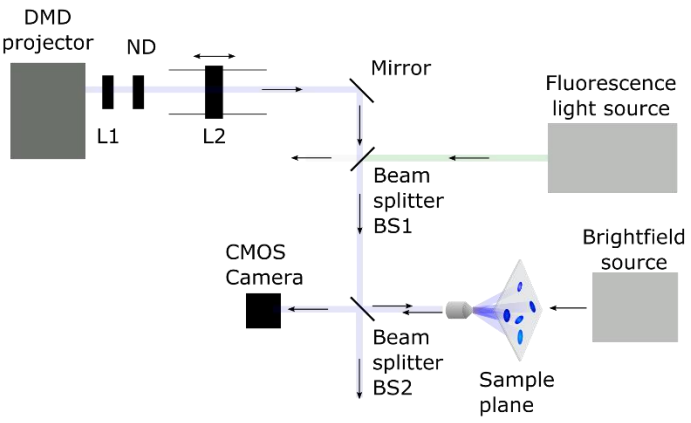

B

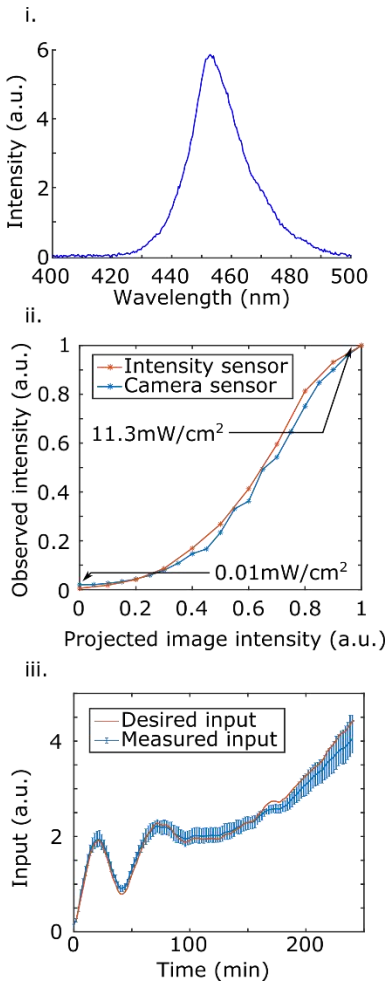

C

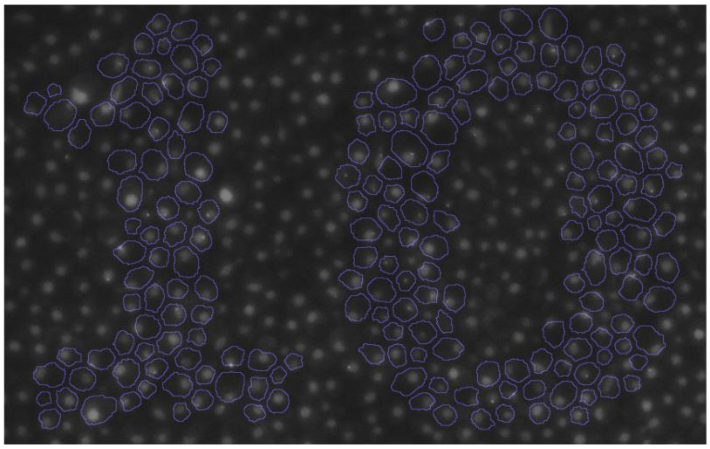

Figure S1. Details on the DMD-based experimental setup for photostimulation, related to Figure 1.

(A) Schematic of optical setup. Light-path from the DMD projector (blue) to the microscope sample plane. The epifluorescence light-path from the fluorescence light source (green) to the sample plane follows the same path as the light from the DMD projector after beam splitter BS1. L1 and L2 are biconvex lenses (f=25.4mm, f=100mm respectively). L2 is mounted on a support that allows its displacement along the axis parallel to the light-path, for fine-tuning of the image focus. ND is a neutral density filter (optical density of 1.3 for single-cell control, optical density of 2 for all other experiments). The two beam splitters (BS) have a light transmission of 50% in the visible range. All components are listed in Table S3.

(B) Specifications of light delivery system. (i) Spectrum of light emitted by the DMD projector. The spectrum of blue light emitted by the DMD projector was measured at the sample plane by an Ocean Optics USB2000+ spectrometer (Ocean Optics, USA). (ii) Intensity of light at the sample plane as a function of projected image intensity. Blue light was displayed by the DMD projector onto the sample plane, and its intensity quantified using a S170C microscope slide power sensor, together with a PM100USB power meter (Thorlabs). The blue light intensity measured through the power meter (orange) ranged from 0.01mW/cm^2 11.3mW/cm^2. The light reflected from the sample plane back to the microscope camera was also measured by quantifying the average pixel value (blue line). The two approaches show a good correlation. Therefore, light reflected back to the microscope camera can be used to estimate the intensity of light during experiments. (iii) Homogeneity of light intensity across the field of view, and ability to regulate light intensity. The light intensity dictated by the population-level feedback in experiment Figure S4E (orange) is plotted together with the average amount of light reflected by the cells (blue line). Whiskers span from the 5th to the 95th percentile of the distribution of light reflected by the cells. The average light intensity seen by the cells closely tracks the controller output, and the variations in light intensity received by the cells are small. Therefore, the light delivery system can faithfully transmit instructions from the controller to the cell population.

(C) Patterned illumination of a dense yeast micro-colony. Image corresponding to Figure 1D, where selected cells (marked by a blue outline) are targeted with light in order to form the number “10”. This image was captured after 10 min of blue-light illumination, and is composed of maximal intensity projection of 5 fluorescent images (Cy3) spanning 3µm in the z-axis. Cells targeted by light change during the time-course experiment, due to cell movement and cell segmentation errors (see Video S1).

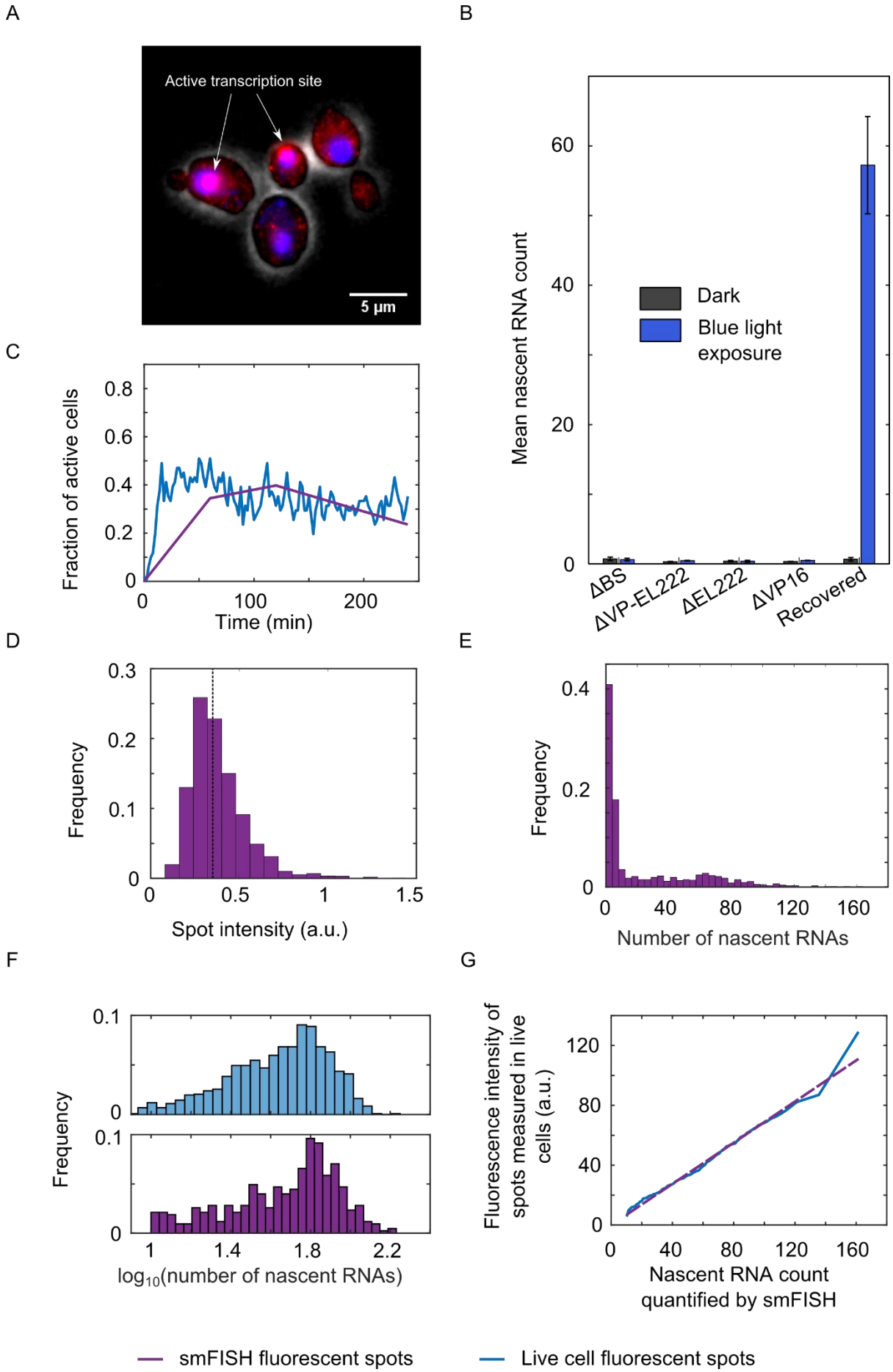
A
Active transcription site
5 µm
B
Mean nascent RNA count
60
40
20
0
Dark
Blue light exposure
ΔBS
ΔVP-EL222
ΔEL222
ΔVP16
Recovered
C
Fraction of active cells
0.8
0.6
0.4
0.2
0
0
100
200
Time (min)
D
Frequency
0.3
0.2
0.1
0
0
0.5
1
1.5
Spot intensity (a.u.)
E
Frequency
0.4
0.2
0
0
40
80
120
160
Number of nascent RNAs
F
Frequency
0.1
0
0.1
0
1
1.4
1.8
2.2
log10(number of nascent RNAs)
G
Fluorescence intensity of spots measured in live cells (a.u.)
120
80
40
0
0
40
80
120
160
Nascent RNA count quantified by smFISH
smFISH fluorescent spots
Live cell fluorescent spots

Figure S2. Calibration of nascent RNA counts by smFISH, related to Figure 1 and 2.

(A) Representative microscopy image of the smFISH experiment. Cells were grown under blue light illumination (420 μW/cm^2) for 2 hour and smFISH was performed with CY3 labeled probes complementary to the PP7 stem-loop. Grayscale: phase contrast / cell boundaries (smoothed using a median filter), blue: DAPI channel (maximum intensity z-projection), red: CY3 channel (maximum intensity z-projection).

(B) Light-dependent induction of transcription requires the expression of VP-EL222 and the presence of its cognate binding sites in the target promoter. The transcriptional response of multiple strains was characterized by growing cells in the dark for 20 min (grey) and subsequently under blue light exposure for 40 min (blue; same light intensity used in Figure 2A, red line). Strains contain the following modifications but are otherwise equivalent to DBY96, the strain used for most experiments in this study (see Methods for details on strain construction). ΔBS expresses the reporter gene under control of the CYC180 sequence without EL222 binding sites. ΔVP-EL222 is deleted for VP-EL222. ΔEL222 and ΔVP16 are based on ΔVP-EL222 and expresses NLS-VP16 and NLS-EL222, respectively. We reintroduced the VP-EL222 construct into ΔVP-EL222 to show that the lack of transcriptional response is specific to the VP-EL222 deletion ("Recovered"). The transcriptional response of the cells was measured in 2 min intervals with the image acquisition and image processing pipeline described in the Methods. The number of nascent RNAs per cell were averaged over all cells and frames for each condition, in order to obtain the mean nascent RNA count under no light exposure (grey bar), and under blue light exposure (blue bar). Data represent the mean and s.d. of two independent experiments.

(C) Comparison of the transcriptionally active cell fraction in a smFISH (purple) and a live-cell (blue) experiment. For technical reasons, smFISH experiments were performed in culture tubes (see Methods) making the direct adjustment of corresponding light intensities between the two types of experiments challenging. The figure shows results for illumination conditions under which the cellular response is comparable for both smFISH and live-cell experiments. The distributions of nascent RNA measurements of these experiments is used for the calibration shown in (E) and (F).

(D) Fluorescence intensity of single cytoplasmic spots corresponding to individual mRNA molecules. 3110 spots were identified and quantified in cells illuminated for one hour with blue light (210 μW/cm^2). Under these conditions, single mRNAs can be readily identified due to their low copy numbers per cell. The median spot intensity is marked in the plot and was used for the calibration of nascent RNA counts for smFISH experiments.

(E) Distribution of nascent RNA counts quantified by smFISH for cells grown under blue light illumination (420 μW/cm^2) for 2 hours.

(F) Distribution of nascent RNA count extracted from live-cell (top) and smFISH (bottom) experiments shown in (B), in logarithmic scale. The distribution of live-cell measurements has been scaled to match the quantiles of the smFISH distribution. In this manner, fluorescence measurements in live cells can be translated to absolute nascent RNA counts. Nascent RNA counts lower than 10 as quantified by smFISH were excluded from this analysis, as that is the detection limit determined for the live-cell quantification. The full nascent RNA count distribution quantified by smFISH is shown in (D).

(G) Quantile-quantile plot from the live-cell and smFISH distributions shown in (E). The quantiles of the nascent RNA count distributions from live-cell and smFISH measurements are plotted against each other. The approximate linearity between the plotted variables indicates that the two distributions have a similar shape. The slope of line indicates the proportionality constant between the fluorescence units from the live-cell measurements and the total nascent RNA counts from the smFISH experiment.

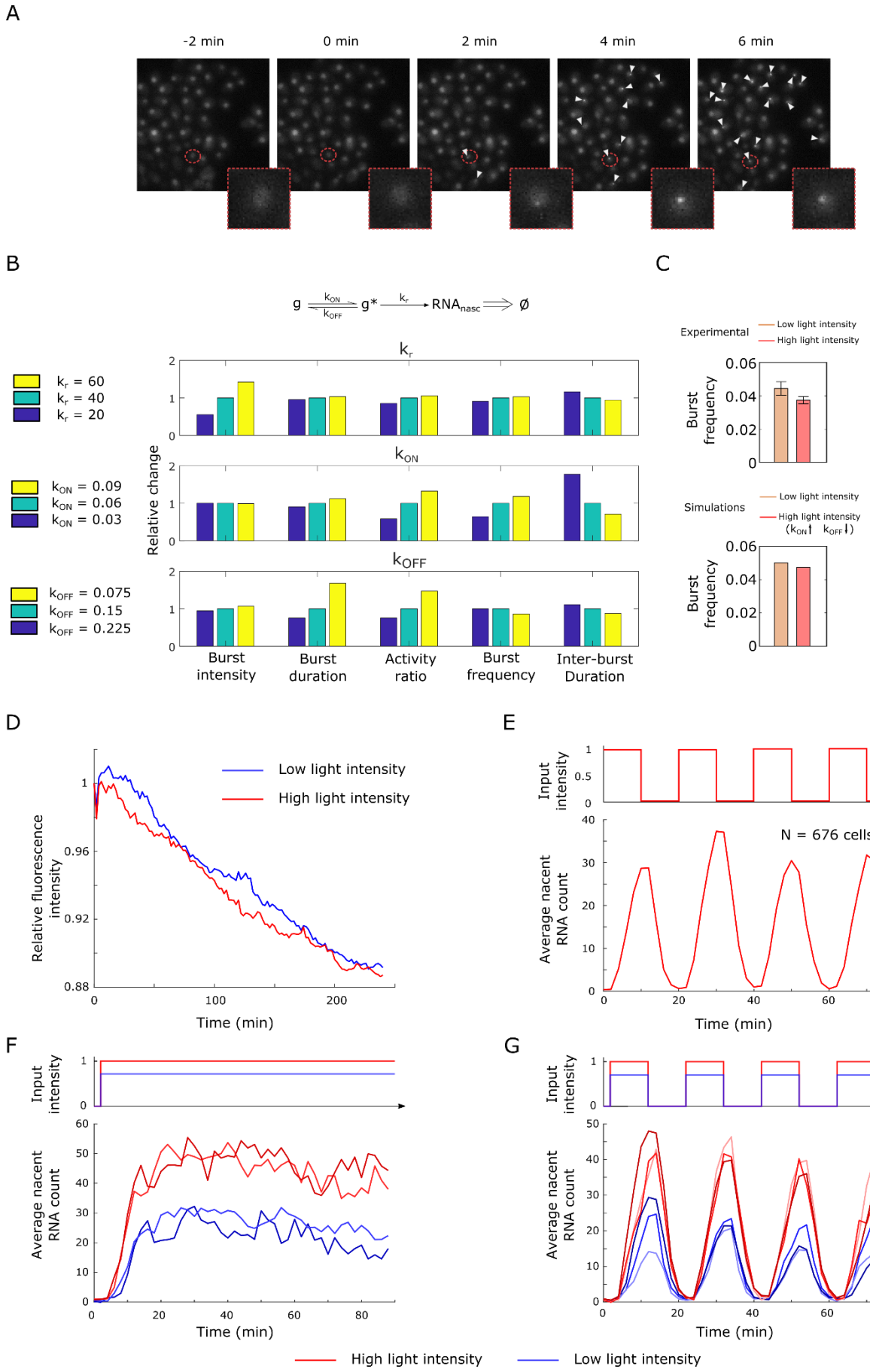
A
-2 min
0 min
2 min
4 min
6 min
B
g ⇌ g* → RNA_nascent → ∅
k_ON
k_OFF
k_r
k_r = 60
k_r = 40
k_r = 20
k_ON = 0.09
k_ON = 0.06
k_ON = 0.03
k_OFF = 0.075
k_OFF = 0.15
k_OFF = 0.225
Relative change
Burst intensity
Burst duration
Activity ratio
Burst frequency
Inter-burst Duration
C
Experimental
Low light intensity
High light intensity
Burst frequency
Simulations
Low light intensity
High light intensity (k_ON ↑ k_OFF ↓)
Burst frequency
D
Low light intensity
High light intensity
Relative fluorescence intensity
Time (min)
E
Input intensity
N = 676 cells
Average nacent RNA count
Time (min)
F
Input intensity
Average nacent RNA count
Time (min)
G
Input intensity
Average nacent RNA count
Time (min)
High light intensity
Low light intensity

Figure S3. Analysis of transcriptional dynamics, related to Figure 2 and Figure 3.

(A) Time-lapse microscopy of transcription activation. Representative images (RFP channel) showing the initial transcriptional response of cells exposed to constant blue light. Time before or after the start of illumination is shown above the individual images. Fluorescent spots, corresponding to nascent RNAs at the transcription site, are marked by white arrowheads. The insets show a close-up of the cell marked with red in the main image. This cell shows nascent RNA accumulation 2 min after illumination.

(B) Sensitivity of burst metrics to the model parameters. A stochastic model of transcription (top) is used to evaluate the influence of model parameters on burst intensity, burst duration, inter-burst duration, activity ratio, and burst frequency (number of bursts per min). Model parameters are varied one at a time by increasing their nominal value by 50%, or decreasing it by 50%.

(C) Effect of light intensity on burst frequency. Data corresponding to Figure 2A. (Top) Cells were exposed to constant blue light of high (red) or low (orange) intensity. The burst frequency, defined as number of transcriptional bursts per minute, was calculated for each cell trace and then averaged over all cells exposed to a given light intensity. Whiskers indicate s.d. of two independent experiments. (Bottom) Simulations of the 2-state promoter model described in B, where k_{on} is increased and k_{off} is decreased for the high light intensity condition (red).

(D) Evaluation of photobleaching during time-lapse experiments. Mean relative fluorescence intensity over time of cells under high (red) or low (blue) light intensity. Fluorescence intensity of each cell was quantified with CellX (Dimopoulos et al., 2014). Average fluorescence was normalized by the fluorescence at the second timepoint.

(E) Demonstration of throughput capabilities of the experimental platform. A large number of cells (676) was exposed to four pulses of high intensity blue light (top). The transcriptional response of each cell was quantified over the whole experiment (bottom). The average nascent RNA count per timepoint is shown.

(F) Transcriptional response to constant light. Data corresponding to Figure 2A. (Top) Cells were exposed to constant blue light of high (red) or low (blue) intensity. (Bottom) Average nascent RNA count of the cell population, with each line representing data from an independent experiment (47 and 171 cells for low intensity light, 47 and 56 for high intensity light). The color tonality of the lines changes slightly to be able to differentiate the different experiments.

(G) Transcriptional response to a sequence of light pulses. Data corresponding to Figure 2B. (Top) Cells were exposed to pulses of low (blue) and high (red) intensity blue light with a duration and an interpulse interval of 10 min. (Bottom) Average nascent RNA count of the cell population, with each line representing data from an independent experiment (342, 117 and 494 cells for low intensity light, 226, 51 and 324 cells for high intensity light). The color tonality of the lines changes slightly to be able to differentiate the different experiments.

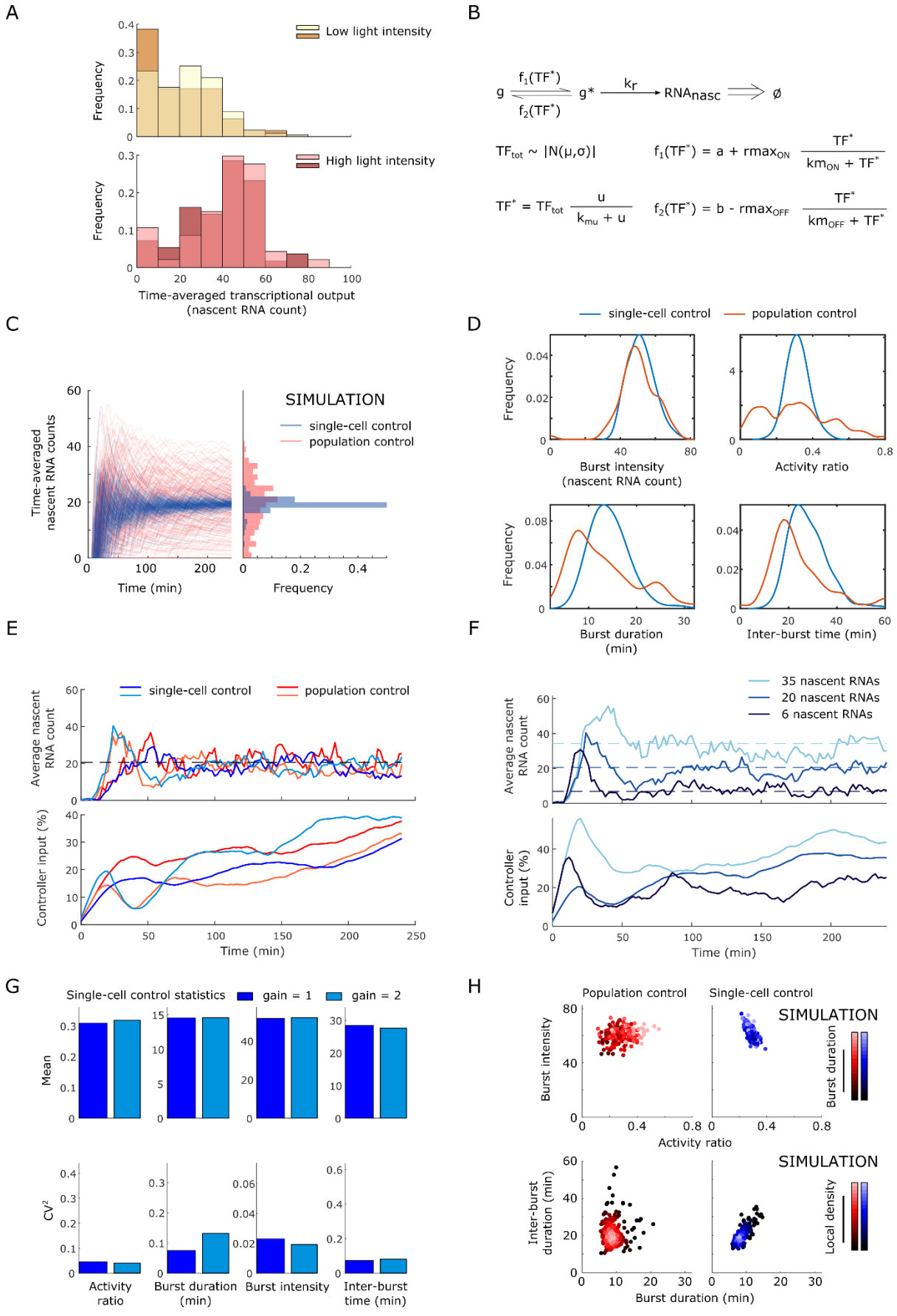
A
Low light intensity
High light intensity
Frequency
Time-averaged transcriptional output
(nascent RNA count)
B
g
f1(TF*)
f2(TF*)
g*
kr
RNAnasc
ø
TFtot ~ |N(μ,σ)|
f1(TF*) = a + rmaxON TF* / kmON + TF*
TF* = TFtot u / kmu + u
f2(TF*) = b - rmaxOFF TF* / kmOFF + TF*
C
SIMULATION
single-cell control
population control
Time-averaged nascent RNA counts
Time (min)
Frequency
D
single-cell control
population control
Frequency
Burst intensity (nascent RNA count)
Activity ratio
Burst duration (min)
Inter-burst time (min)
E
single-cell control
population control
Average nascent RNA count
Controller input (%)
Time (min)
F
35 nascent RNAs
20 nascent RNAs
6 nascent RNAs
Average nascent RNA count
Controller input (%)
Time (min)
G
Single-cell control statistics
gain = 1
gain = 2
Mean
CV²
Activity ratio
Burst duration (min)
Burst intensity
Inter-burst time (min)
H
Population control
Single-cell control
SIMULATION
Burst intensity
Activity ratio
Burst duration
Inter-burst duration (min)
Burst duration (min)
Local density

Figure S4. Further details on feedback experiments, related to Figure 4 and 5.

(A) Time-averaged transcriptional response varies among cells. Histograms of the time-averaged transcriptional response of cells exposed to low intensity light (top), or high intensity light (bottom) for 90 min (Figure 2A).

(B) Extended stochastic model of transcription. Equations used to extend the stochastic model presented in Figure 3D (Methods). Parameter values are found in Table S4

(C) Simulation comparing the ability of single-cell control and population control to reduce differences in transcriptional output between cells. The extended stochastic model is used to simulate the time-averaged transcriptional response of cells under population control (red) or single-cell control (blue). (Left) Thin lines are single-cell time-averages. (Right) Distribution of time-averaged nascent RNA counts over the experiment duration for each cell.

(D) Density approximation of the distribution of each burst metric, extracted from cells under population-level feedback (orange) or single-cell feedback (blue). Mean burst intensity, mean burst duration, mean inter-burst duration, and activity ratio were extracted from each cell trace. The histogram of these four metrics was then smoothed using a kernel smoothing function to obtain the shown distributions.

(E) Comparison of population and single-cell integral feedback control. Data corresponding to Figure 4B, and Figure 5. (Top) The nascent RNA count averaged over all cells at each timepoint is plotted against time (thick lines, 44 and 88 cells for population control, 98 and 114 cells for single-cell control). Blue lines correspond to single-cell control experiments with weak (dark blue) or strong (light blue) feedback gain. Red lines correspond to the mean behavior of cells under population control. The dashed black line indicates the pre-specified target nascent RNA count common for all experiment. (Bottom) Average input given to the cells at each timepoint.

(F) Single cell control tracks constant references. Data corresponding to Figure 4C. (Top) The nascent RNA count averaged over all cells at each timepoint is plotted against time (thick lines, 70 cells for the lowest setpoint, 114 cells for the intermediate setpoint, 104 cells for the highest setpoint). Dashed lines indicate the pre-specified target nascent RNA count for each experiment. (Bottom) Average input given to the cells at each timepoint.

(G) Changes in single-cell feedback gain do not affect transcription dynamics of the controlled cells. Mean burst intensity, mean burst duration, mean inter-burst time, and activity ratio were extracted from each cell trace. Mean and CV^2 of each of these metrics were computed for the two controller gains used in this study. The mean and standardized variance of all burst metrics are approximately equal for the two controller gains. Thus, pooling cell traces under single-cell control with feedback gains in this range does not influence our analysis of transcription dynamics.

(H) Computer simulations of single-cell and population control using the two-state promoter model without extrinsic noise cannot reproduce the experimental observations. Model predictions made for population control (left side, red color) and single-cell control (right side, blue color) on the relationship between the different burst metrics. Each dot corresponds to statistics calculated from a single cell trace. (Top) The mean burst intensity of each cell is plotted against the cell's activity ratio. Color intensity indicates mean burst duration. (Bottom) The mean burst duration of each cell is plotted against the cell's inter-burst length. The model simulations do not reproduce the negative correlation between these two burst metrics observed

experimentally for population control (Figure 5B). Color intensity is proportional to the local density of dots in the plot.

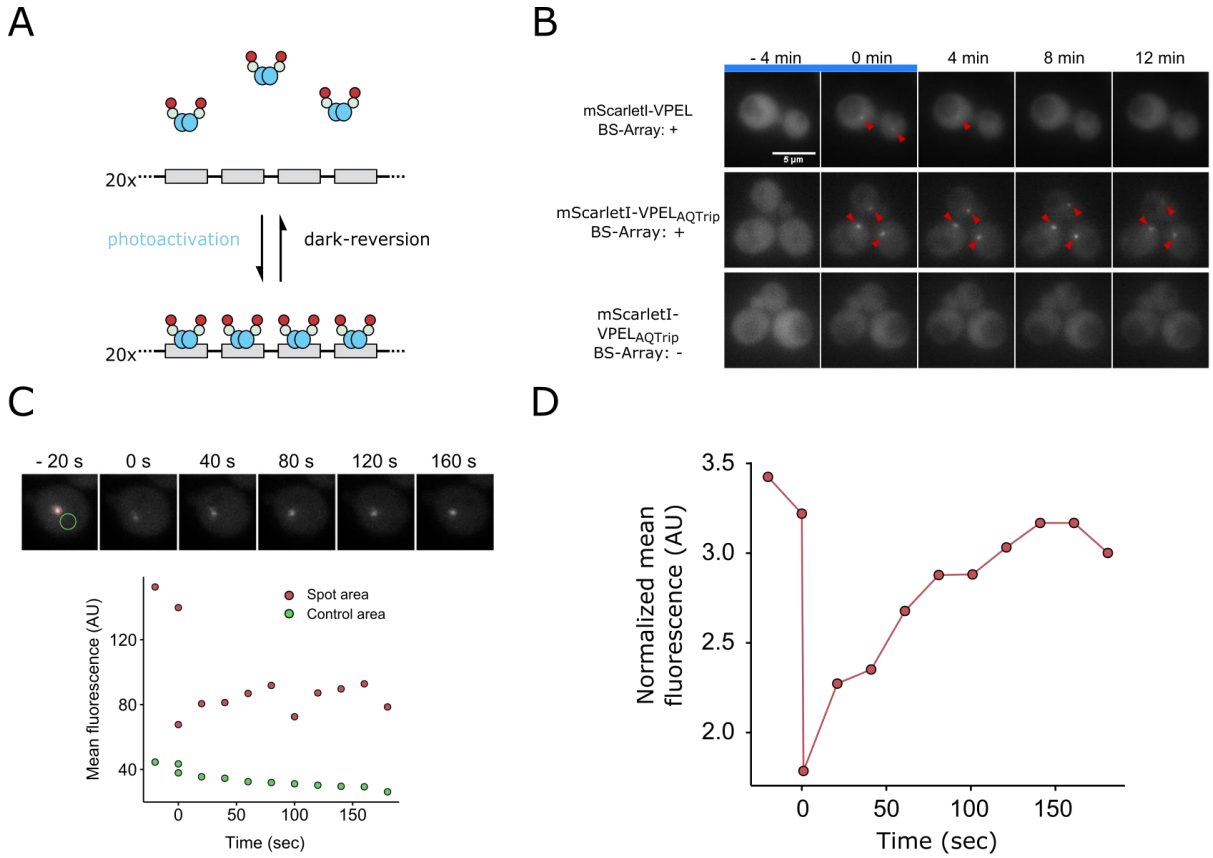
A
20x
photoactivation
dark-reversion
20x
B
- 4 min
0 min
4 min
8 min
12 min
mScarletI-VPEL
BS-Array: +
5 µm
mScarletI-VPEL$_{AQTrip}$
BS-Array: +
mScarletI-
VPEL$_{AQTrip}$
BS-Array: -
C
- 20 s
0 s
40 s
80 s
120 s
160 s
Spot area
Control area
Mean fluorescence (AU)
120
80
40
0
50
100
150
Time (sec)
D
Normalized mean
fluorescence (AU)
3.5
3.0
2.5
2.0
0
50
100
150
Time (sec)
E
VPEL$_{fluor}$ + BS
k_{on}
k_{off}
Complex$_{fluor}$
561
laser
VPEL$_{dark}$ + BS
k_{on}
k_{off}
Complex$_{dark}$
F
VPEL: 800
inferred k_{off} : 0.0192 s^{-1}
VPEL: 1600
inferred k_{off} : 0.018 s^{-1}
VPEL: 6400
inferred k_{off} : 0.0168 s^{-1}
k_{on} (s^{-1})
0.015
0.010
0.005
0.01
0.02
0.03
0.04
k_{off} (s^{-1})
ln(SSE) :
-2
-4
-6
G
Avg inter-burst
duration (min)
40
20
0
0.1
0.3
0.5
0.7
Activity ratio
Avg burst
intensity
60
30
0
0.1
0.3
0.5
0.7
Activity ratio
experimental
data
k_c = 125
k_c = 25
k_c = 75
k_c = 1

Figure S5. Details of FRAP experiments, related to Figure 6.

(A) Schematic representation of mScarletI-VP-EL222 recruitment to an array of 80 binding sites.

(B) Recruitment of mScarletI tagged VP-EL222 upon 4 min of blue light illumination (performed using a 5 sec light pulse every 30 sec). Representative fluorescence microscopy images are shown for strains containing the binding site array and expressing either mScarletI tagged VP-EL222 (top) or its mutant AQTrip (middle). Further, a control experiment using a strain without binding sites is shown (bottom). Time is indicated relative to the end of the illumination period. Fluorescent foci are marked with red arrowheads. The data shows the prolonged presence of fluorescent foci for VP-EL222-AQTrip resulting from the stabilized photoactivated state. This mutant was used during FRAP experiments to avoid dark-state reversion.

(C) Non-normalized example data for FRAP experiment of a single cell. Fluorescence microscopy images (mScarletI) are shown (top). Time is indicated relative to the photobleaching event. Regions used to quantify the spot (red circle) and background fluorescence for normalization (green circle) are indicated in the first image. The mean fluorescence over time of pixels in these regions are shown (bottom). Regions were adjusted manually between timepoints.

(D) Normalized FRAP data of the single cell shown in C. Mean fluorescence of the spot area was divided by the mean fluorescence of the control.

(E) Schematic representation of the ODE model used to analyze the FRAP experiment. The model describes the binding and unbinding of fluorescent and dark VP-EL222 ($VPEL_{fluor}$, $VPEL_{dark}$) to its binding sites (BS) with rate k_{on} and k_{off}. Photobleaching is modeled by converting $Complex_{fluor}$ to $Complex_{dark}$ (representing BSs bound by either fluorescent or dark VP-EL222) to match the relative fluorescence derived from experimental spot data pre- and post-bleaching.

(F) Evaluation of FRAP model parameters. Parameters k_{on} and k_{off} were varied and the logarithm of the sum of squared errors between model and data (see Figure 4B) is plotted. A further unknown parameter is the initial condition for $VPEL_{fluor}$. By measuring integrated fluorescence values in the spot area and comparing it to the value of the whole cell, we find that the spot area makes up for 5% of the total cellular fluorescence. This results in an estimated copy number of 1600 molecules for $VPEL_{fluor}$, assuming that all binding sites of the array are bound. Due to this number being a rough estimate, we evaluated how the initial conditions of $VPEL_{fluor}$ (indicated above the respective plots) affect the estimated value of k_{off}. We found that k_{off} changes less than 15% for an 8-fold change in $VPEL_{fluor}$ initial conditions, indicating that the results of the analysis are not very sensitive to the initial condition of $VPEL_{fluor}$.

(G) Comparison of observed burst intensity and inter-burst duration to model predictions. Stochastic simulations of the model shown in Figure 6C were used to obtain the relationship between activity ratio and inter-burst duration (left), and between activity ratio and burst intensity (right). Simulation results are represented by solid lines, while points indicate the mean and SEM of experimental data. The experimental data was obtained by binning cell traces from Figure 2A according to their activity ratio, and then computing the average burst intensity and inter-burst duration for cells in each bin. The parameter k_c determines the rate of the first TF binding event ($k_{on}' = k_{on} / k_c$), with greater values of k_c indicating a smaller binding affinity.

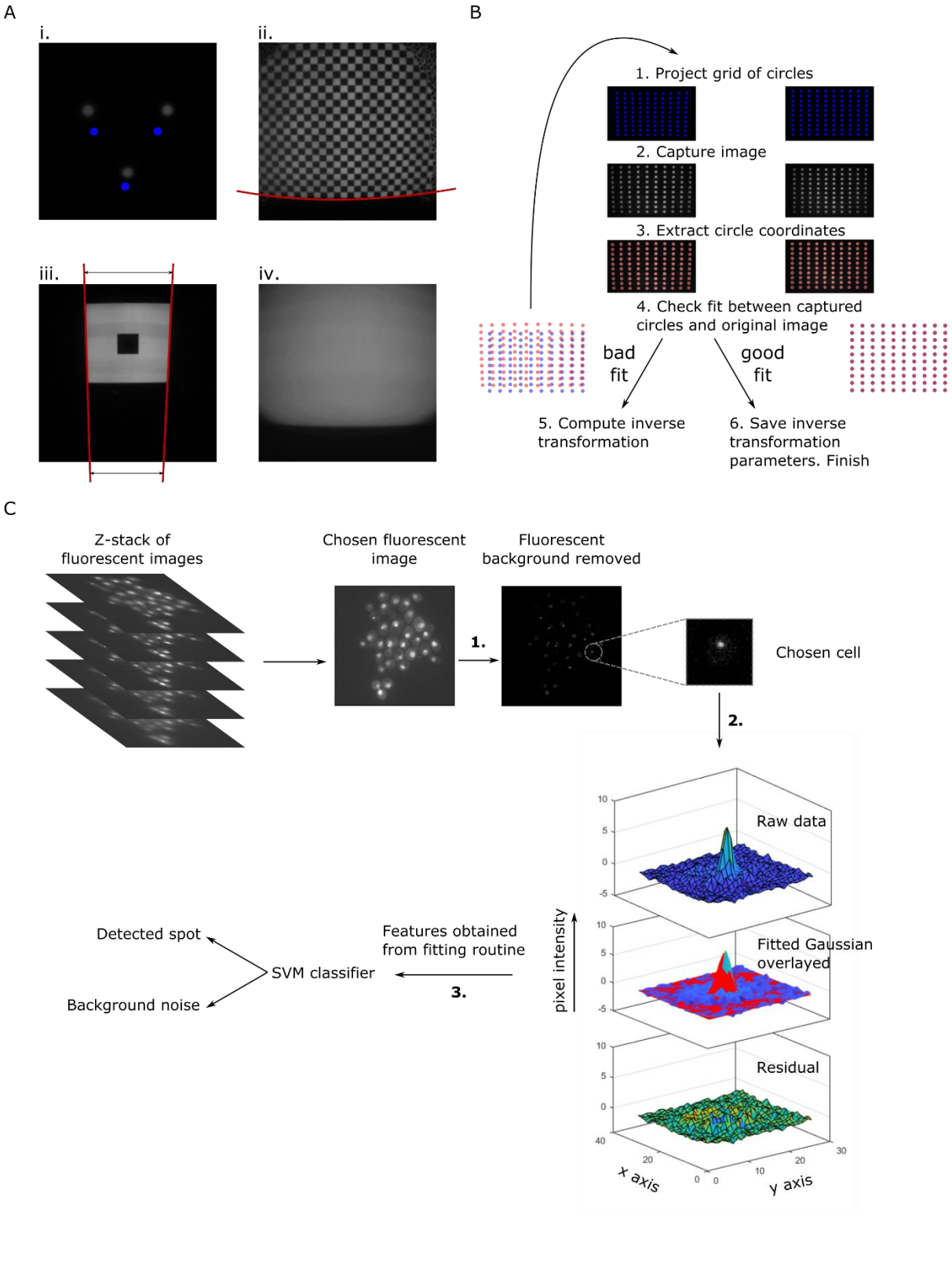
A
i.
ii.
iii.
iv.
B
1. Project grid of circles
2. Capture image
3. Extract circle coordinates
4. Check fit between captured circles and original image
bad fit
good fit
5. Compute inverse transformation
6. Save inverse transformation parameters. Finish
C
Z-stack of fluorescent images
Chosen fluorescent image
Fluorescent background removed
1.
Chosen cell
2.
Raw data
Fitted Gaussian overlayed
Residual
pixel intensity
x axis
y axis
Features obtained from fitting routine
3.
SVM classifier
Detected spot
Background noise

Figure S6. Calibration of light delivery system and nascent RNA quantification, related to STAR Methods

(A) Distortions present in the images projected onto the microscope sample plane. (i) Scale and shift. Three circles are projected onto the sample plane. The projected image (blue) is scaled and shifted when imaged at the sample plane (gray). (ii) Barrel distortion. A checkers pattern is projected onto the field of view (gray). The bottom of the image is warped, as indicated by the red line. (iii) Perspective distortion. A square shape is projected onto the sample plane. The image captured (gray) shows the distortions introduced to the square, which appears as a trapezoid. (iv) Vignetting (uneven illumination). Uniform light intensity is projected onto the field of view. When imaged (gray), pixel intensity decreases as a function of the distance to the image center.

(B) Software alignment of light delivery system. An automated routine for the removal of distortions described in A is run at the start of every experiment. First, a regular grid of points is projected onto the field of view (1), and is imaged (2). The coordinates of the projected points are extracted and compared to the original image (3). If both sets of points match, the procedure is finished. Else, a function that maps DMD projector pixels to camera pixels is fit, its inverse applied to the original grid of points, and the procedure restarted at step (1). After distortions (i)-(iii) have been compensated, the vignetting effect is removed. An image of uniform intensity is projected, and the element-wise inverse of the captured image is used as a correction matrix.

(C) Workflow for nascent RNA quantification. A z-stack of fluorescent images spanning 3µm is taken in order to capture the cells' active transcription sites, which might lie at different z-positions inside the nucleus. Each image is passed through the nascent RNA quantification pipeline. First, background fluorescence is removed (1). Then, a rectangular box around each cell is used to crop the image. A 2D gaussian function sitting on a tilted plane is fitted to the pixel intensity profile of the cropped image (2). The volume of the fitted function is used as the spot intensity, proportional to the number of nascent RNAs. As this procedure is applied to every cell, non-transcribing cells will get assigned a positive number of nascent RNAs. To correct for this, we pass features from the fitting routine to a binary classifier (3), which decides whether the analyzed cell is actively transcribing or not. In the latter case, nascent RNA count is set to 0.

Supplementary Table 1. Plasmids used for strain construction, related to STAR methods. Promoters are represented by 'pr', terminators are represented by 'term'.

Plasmid	Backbone	Insert	Source
pDB58	pKERG105	*ACT1*pr-VPEL222-*CYC1*term	Manuscript under review
pDB96	pDZ306	*GLT1*-5xELbs-*CYC180*pr-24xPP7SL	this study
pDB97	pRG205	*MET25*pr-tdPCP-NLS-tdmRuby3-*CYC1*term	this study
pDB81	pKERG105	80-EL-BS-Array	this study
pDB145	pKERG106	*ACT1*pr-mScarletI-*CYC1*term	this study
pDB146	pKERG106	*ACT1*pr-mScarletI-VPEL222(AQTrip)-*CYC1*term	this study
pDB147	pKERG105	*ACT1*pr-NLS-VP16-*CYC1*term	this study
pDB148	pKERG105	*ACT1*pr-NLS-EL222-*CYC1*term	this study

Supplementary Table 2. Strains used in this study, related to STAR methods. Promoters are represented by 'pr', terminators are represented by 'term'.

Name	Genotype	Source
BY4741	*MAT**a** his3Δ1 leu2Δ0 met15Δ0 ura3Δ0*	Euroscarf
BY4742	*MAT**alpha** his3Δ1 leu2Δ0 lys2Δ0 ura3Δ0*	Euroscarf
DBY41	BY4741, *LEU2*::*ACT1*pr-VPEL222-*CYC1*term(pDB58)	manuscript under review
DBY80	DBY41, *GLT1*prΔ::*HIS3*-5xELbs-*CYC180*pr-24xPP7SL(pDB96)	this work

DBY91	BY4742, *URA3*::*MET25*pr-tdPCP-NLS-tdmRuby3-*CYC1*term(pDB97)	this work
DBY96	DBY80 mated with DBY91	this work
DBY132	BY4741, *GLT1*prΔ::*URA3MX*-*CYC180*pr-24xPP7SL, *LEU2*::*ACT1*pr-VPEL222-*CYC1*term	this work
DBY133	BY4741, *GLT1*prΔ::HIS3-5xELbs-*CYC180*pr-24xPP7SL(pDB96), *LEU2*::*ACT1*pr-NLS-URA3MX-*CYC1*term	this work
DBY134	DBY91, *LEU2*::*ACT1*pr-VPEL222-*CYC1*term(pDB58)	this work
DBY135	DBY91, *LEU2*::*ACT1*pr-NLS-VP16-*CYC1*term(pDB147)	this work
DBY136	DBY91, *LEU2*::*ACT1*pr-NLS-EL222-*CYC1*term(pDB148)	this work
DBY138	DBY132 mated with DBY91	this work
DBY139	DBY133 mated with DBY91	this work
DBY140	DBY133 mated with DBY134	this work
DBY141	DBY133 mated with DBY135	this work
DBY142	DBY133 mated with DBY136	this work
DBY30	BY4742, *LEU2*::80-EL-BS-Array(pDB30)	this work
DBY144	DB30, *URA3*::*ACT1*pr-mScarletI-VPEL-*CYC1*term(pDB145)	this work
DBY145	DB30, *URA3*::*ACT1*pr-mScarletI-VPEL(AQTrip)-*CYC1*term(pDB146)	this work
DBY146	DBY4741, *URA3*::*ACT1*pr-mScarletI-VPEL(AQTrip)-*CYC1*term(pDB146)	this work

Supplementary Table 3. Optical components composing the light delivery system, related to STAR methods. All parts were bought from Thorlabs, with the exception of the beam splitters (AHF analysentechnik, Germany)

	Part Number	Item Description	Quantity
Lenses	LB1761-A	Bi-Convex Lens 1" f = 25.4mm	1
	LB1630-A	Bi-Convex Lens 2" f = 100mm	1
Lense mounting	LCP01/M	60 mm Cage Plate	2
	CP02	30 mm Cage Plate	2
Cage mounting	ER8-P4	Cage Assembly Rod 8"	4
	ER3-P4	Cage Assembly Rod 3"	4
	LCP02/M	30mm to 60mm Cage Plate Adapter	1
	TR150/M	Optical Post L = 150mm	2
	UPH100/M	Universal Post Holder L = 100mm	2
Neutral density filter	NE20B	25 mm Absorptive ND Filter Optical Density: 2	1
	NE13B	25 mm Absorptive ND Filter Optical Density: 1.3	1
Beam splitter	F21-000	50R/50T beam splitter	2

Supplementary Table 4. Parameter values for the stochastic gene expression model, related to STAR methods. Time units are minutes, abundance units are molecular counts.

Parameter	Value
k_r	40
k_{ON}	0.06
k_{OFF}	0.15
μ	1
σ	0.5
km_U	0.2
a	0
$rmax_{ON}$	5
km_{ON}	0.2
b	0.3
$rmax_{OFF}$	0.27
km_{off}	0.05